Inorg. Chem. **2009**, *48*, 1871−1878

Mechanism of the Divanadium-Substituted Polyoxotungstate $[\gamma\text{-}1,2\text{-}H_2SiV_2W_{10}O_{40}]^{4-}$ Catalyzed Olefin Epoxidation by H_2O_2: A Computational Study

Aleksey E. Kuznetsov, Yurii V. Geletii, Craig L. Hill, Keiji Morokuma, and Djamaladdin G. Musaev*

Cherry L. Emerson Center for Scientific Computation and Department of Chemistry, Emory University, 1515 Dickey Drive, Atlanta, Georgia 30322

Received July 22, 2008

The mechanisms of olefin epoxidation by hydrogen peroxide catalyzed by $[\gamma\text{-}1,2\text{-}H_2SiV_2W_{10}O_{40}]^{4-}$, **1**, were studied using the density functional (B3LYP) approach in conjunction with large basis sets. The role of solvent is taken into account via both including an explicit water molecule into the calculations and using the polarizable continuum model (PCM) with acetonitrile as a solvent (numbers given in parentheses). The countercation effect (using one molecule of Me_4N^+ as a countercation (1CC)) is also taken into account (numbers given in brackets). It was shown that the formation of the vanadium-hydroperoxo species **2(H$_2$O)** with an {OV-(μ-OOH)(μ-OH)-VO}(H_2O) core from **1** and H_2O_2 is a very facile process. The resulting complex **2(H$_2$O)** may eliminate a water molecule and form complex **2**. From the intermediates **2** and **2(H$_2$O)**, reaction may proceed via two distinct pathways: "hydroperoxo" and "peroxo". The water-assisted "hydroperoxo" pathway starts with coordination of olefin (C_2H_4) to **2(H$_2$O)** and proceeds with a 36.8(25.5)[31.7][(21.6)] kcal/mol rate-determining barrier at the O-atom transfer transition state **TS2[TS2$_{1CC}$]**. The "water-free peroxo" and "water-assisted peroxo" pathways start with rearrangement of **2** and **2(H$_2$O)** to vanadium-peroxo species **3** and **3(H$_2$O),** respectively, with an {OV-(η^2-O_2)-VO} core, and follow the O-atom transfer from catalyst to olefin. The **2** → **3** and **2(H$_2$O)** → **3(H$_2$O)** hydroperoxo → peroxo rearrangement processes require 16.8(13.0)[13.0][(11.1)] and 14.2(9.0)[1.3][(7.2)] kcal/mol of energy, respectively. The calculated overall energy barriers are 28.1(19.1)[23.8][(17.2)] and 25.4(11.0)[10.6][(13.0)] kcal/mol for "water-free peroxo" and "water-assisted peroxo" pathways, respectively. On the basis of these data we predict that the $[\gamma\text{-}1,2\text{-}H_2SiV_2W_{10}O_{40}]^{4-}$-catalyzed olefin epoxidation by H_2O_2 most likely occurs via a "water-assisted peroxo" pathway.

I. Introduction

Catalytic epoxidation of olefins has received considerable attention because of importance of epoxides as raw materials for the production of paints, epoxy resins, and surfactants.[1,2] Over the years, a number of environmentally hazardous epoxidation processes that utilize a variety of catalysts and oxidants have been developed. The use of hydrogen peroxide as an oxidant offers an environmentally and economically attractive alternative;[3,4] it is cheap, has the second highest active oxygen content (after the oxygen molecule), and produces water as an only by-product. In the literature, several catalysts with high-valent early transition metals such as Ti(IV), W(VI), V(V), and Re(VII) have been reported to be effective for the epoxidation of alkenes with H_2O_2,[5] among which the recently reported Vanadium(V)-catalyst is very promising. Indeed, the divanadium-substituted polyoxotungstate $[\gamma\text{-}1,2\text{-}H_2SiV_2W_{10}O_{40}]^{4-}$ (**I**) catalyst that contains an {OV-(μ-OH)$_2$-VO} core catalyzes the epoxidation of unactivated aliphatic terminal C_3-C_{10} alkenes including propene with very high yields, with ≥99% selectivity and ≥87% efficiency of H_2O_2 utilization.[6−11] The epoxidation of *cis*- and *trans*-2-octenes gave *cis*-2,3-epoxyoctane (90% yield) and *trans*-2,3-epoxyoctane (6% yield), respectively. This system requires only 1 equiv of hydrogen peroxide with respect to the alkene and produces the epoxide with high yield, stereospecificity, diastereoselectivity, and regioselectivity. It was shown the following: (1) no epoxidation of alkenes proceeded in the absence of **I** or when *tert*-butylhydroperoxide (TBHP) was used as an oxidant;[6] (2) ^{51}V

* To whom correspondence should be addressed. E-mail: dmusaev@emory.edu.

(1) Sheldon, R. A.; Kochi, J. K. *Metal-Catalyzed Oxidations of Organic Compounds*; Academic Press: New York, 1981.
(2) Tullo, A. *Chem. Eng. News.* **2004**, *82*, 15.

10.1021/ic801372j CCC: $40.75
Published on Web 01/28/2009

Scheme 1. Schematic Presentation of the Proposed "hydroperoxo", "water-free peroxo", and "water-assisted peroxo" Pathways of the Reaction $[\gamma\text{-}1,2\text{-}H_2SiV_2W_{10}O_{40}]^{4-} + H_2O_2 + \text{Olefin} \rightarrow [\gamma\text{-}1,2\text{-}H_2SiV_2W_{10}O_{40}]^{4-} + H_2O + \text{Epoxide}$[a]

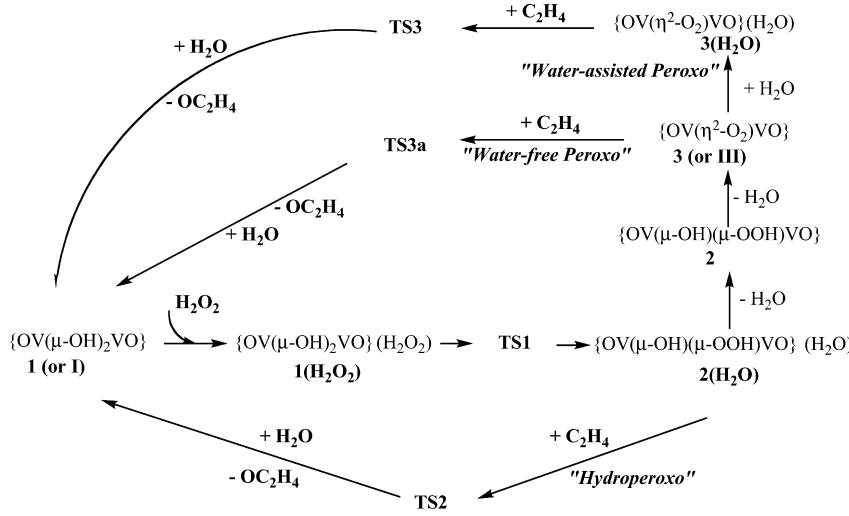

[a] For simplicity, the $[\gamma\text{-}SiW_{10}O_{40}]^{4-}$ unit was omitted.

and ^{183}W NMR studies of the compound **I** recovered after epoxidation show no formation of tungstate species such as $[\alpha\text{-}SiW_{12}O_{40}]^{4-}$, $[\gamma\text{-}SiW_{10}O_{34}(H_2O)_2]^{4-}$, $[W_2O_3(O_2)_4(H_2O)_2]^{2-}$, and $[H_nWO_2(O_2)_2]^{(2-n)-}$;[10] (3) mono- and trivanadium-substituted compounds, $[\alpha\text{-}SiVW_{11}O_{40}]^{5-}$ and $[\alpha-1,2,3\text{-}SiV_3W_9O_{40}]^{7-}$, are catalytically inactive, suggesting that the V−O−W and V=O centers are not the active sites in catalysis;[6,9,10] (4) the silicotungstates $[\gamma\text{-}SiW_{12}O_{40}]^{4-}$ with the same structure as **I** are catalytically inactive, suggesting that the W atoms in **I** are not the active sites;[9,10] (5) the esterification of a bis(μ-hydroxo) dioxovanadium site in $[\gamma\text{-}H_2SiV_2W_{10}O_{40}]^{4-}$ with alcohols is sterically controlled; the secondary and tertiary alcohol esters were hardly formed (equilibrium constant <0.01), and a large equilibrium constant of 75 was observed for the reaction with methanol;[7] and (6) the formation of hydroperoxy intermediate $[\gamma\text{-}SiV_2W_{10}O_{38}(\mu\text{-}OH)(\mu\text{-}OOH)]^{4-}$ by the reaction of **I** with H_2O_2 in 1,2-dichloroethane was confirmed by NMR and mass spectroscopy.[6] It was suggested that the {OV-(μ-OH)$_2$-VO} core of **I** is an active site of the catalyst. In the consequent publication, Nakagawa and Mizuno have extended their investigation[11] and have concluded that the reaction of **I** with hydrogen peroxide leads to the reversible formation of a hydroperoxo species $[\gamma\text{-}SiV_2W_{10}O_{38}(\mu\text{-}OOH)(\mu\text{-}OH)]^{4-}$ (**II**), which later rearranges to peroxo complex $[\gamma\text{-}SiV_2W_{10}O_{38}(\mu\text{-}\eta^2,\eta^2\text{-}O_2]^{4-}$ (**III**). Intermediate **III** was proposed to be an active oxidant species (see Scheme 1).

However, the proposed "peroxo" mechanism for **I**-catalyzed olefin epoxidation by hydrogen peroxide is different from the "hydroperoxo" mechanism predicted by Musaev and co-workers[12] for the lacunary polyoxonetalate (POM), $[\gamma\text{-}H_4SiW_{10}O_{36}]^{4-}$, based on the DFT studies. The "hydroperoxo" mechanism, not studied by Nakagawa-Mizuno, could be an alternative mechanism for the **I**-catalyzed olefin epoxidation by hydrogen peroxide. As seen in Scheme 1, the first step of the both pathways (i.e., "hydroperoxo" and "peroxo") is the addition of H_2O_2 to **I** to form a hydroperoxo intermediate **II**. However, the following steps of the "hydroperoxo" and "peroxo" pathways are very different: in the "hydroperoxo" pathway, species **II** is assumed to be an active oxidant that uptakes a substrate and produces epoxide, while in the "peroxo" mechanism, species **II** is proposed to rearrange to the peroxo intermediate **III**, which is considered to be an active oxidant.

(3) (a) Sanderson, W. R. *Pure Appl. Chem.* **2000**, *72*, 1289–1304. (b) Lane, B. S.; Burgess, K. *Chem. Rev.* **2003**, *103*, 2457–2760. (c) Ishii, Y.; Yamawaki, K.; Ura, T.; Yamada, H.; Yishida, T.; Ogawa, M. *J. Org. Chem.* **1988**, *53*, 3587–3593. (d) Neumann, R.; Gara, M. *J. Am. Chem. Soc.* **1995**, *117*, 5066–5074. (e) Mizuno, N.; Nozaki, C.; Kiyoto, I.; Misono, M. *J. Am. Chem. Soc.* **1998**, *120*, 9267–9272. (f) Hill, C. L.; Prosser-McCartha, C. M. *Coord. Chem. Rev.* **1995**, *143*, 407–455. (g) Kozhevnikov, I. V. *Chem. Rev.* **1998**, *98*, 171–198. (h) White, M. C.; Doyle, A. G.; Jacobsen, E. N. *J. Am. Chem. Soc.* **2001**, *123*, 7194–7195. (i) Que, L., Jr. *Science* **1991**, *253*, 273–274. (j) Pestovsky, O.; Stoian, S.; Bominaar, E. L.; Shan, X.; Munck, E.; Que, L., Jr.; Bakac, A. *Angew. Chem., Int. Ed.* **2005**, *44*, 6871–6874. (k) Bukowski, M. R.; Koehntop, K. D.; Stubna, A.; Bominaar, E. L.; Halfen, J. A.; Muenck, E.; Nam, W.; Que, L., Jr. *Science* **2005**, *310*, 1000–1002. (l) MacBeth, C. E.; Golombek, A. P.; Young, V. G., Jr.; Yang, C.; Kuczera, K.; Hendrich, M. P.; Borovik, A. S. *Science* **2000**, *289*, 938–941. (m) Battioni, P.; Renaud, J. P.; Bartoli, J. F.; Reinaartiles, M.; Fort, M.; Mansuy, D. *J. Am. Chem. Soc.* **1988**, *110*, 8462–8470. (n) Notari, B. *Adv. Catal.* **1996**, *41*, 253–334. (o) Romao, C. C.; Kühn, F. E.; Herrmann, W. A. *Chem. Rev.* **1997**, *97*, 3197–3246. (p) Oesz, K.; Espenson, J. H. *Inorg. Chem.* **2003**, *42*, 8122–8124. (q) Vasbinder, M. J.; Espenson, J. H. *Organometallics* **2004**, *23*, 3355–3358. (r) Venturello, C.; Alneri, E.; Ricci, M. *J. Org. Chem.* **1983**, *48*, 3831–3833. (s) Duncan, D. C.; Chambers, R. C.; Hecht, E.; Hill, C. L. *J. Am. Chem. Soc.* **1995**, *117*, 681–691. (t) De Vos, D. E.; Meinershagen, J. L.; Bein, T. *Angew. Chem., Int. Ed.* **1996**, *35*, 2211–2213. (u) Neumann, R. *Prog. Inorg. Chem.* **1998**, *47*, 317–370. (v) Neumann, R.; Dahan, M. *Nature* **1997**, *388*, 353–355. (w) Neumann, R.; Dahan, M. *J. Am. Chem. Soc.* **1998**, *120*, 11969–11976. (x) Nishiyama, Y.; Nakagawa, Y.; Mizuno, N. *Angew. Chem., Int. Ed.* **2001**, *19*, 3751–3753. (y) Okun, N. M.; Anderson, T. M.; Hill, C. L. *J. Am. Chem. Soc.* **2003**, *125*, 3194–3195. (z) Weinstock, I. A.; Barbuzzi, E. M. G.; Wemple, M. W.; Cowan, J. J.; Reiner, R. S.; Sonnen, D. M.; Heintz, R. A.; Bond, J. S.; Hill, C. L. *Nature* **2001**, *414*, 191–195. (aa) Hill, C. L. In *Comprehensive Coordination Chemistry II*; Wedd, A. G., Ed.; Elsevier Science: New York, 2004; Vol. 4, pp 679; (ab) Neumann, R. In *Modern Oxidation Methods*; Bäckvall, J.-E., Ed.; John Wiley & Sons: New York, 2004.

(4) (a) Khavrutskii, I. V.; Musaev, D. G.; Morokuma, K. *J. Am. Chem. Soc.* **2003**, *125*, 13879–13889. (b) Khavrutskii, I. V.; Rahim, R. R.; Musaev, D. G.; Morokuma, K. *J. Phys. Chem. B* **2004**, *108*, 3845–3854. (c) Khavrutskii, I. V.; Musaev, D. G.; Morokuma, K. *Proc. Natl. Acad. Sci. U.S.A.* **2004**, *101*, 5743–5748. (d) Khavrutskii, I. V.; Musaev, D. G.; Morokuma, K. *Inorg. Chem.* **2005**, *44*, 306–315.

To elucidate a question which of these two proposed pathways of the **I**-catalyzed olefin epoxidation by H_2O_2 is the most (kinetically and thermodynamically) favorable, we investigate the both pathways of the reaction

$$[\gamma\text{-}1,2\text{-}H_2SiV_2W_{10}O_{40}]^{4-} + H_2O_2 + \text{olefin} \rightarrow [\gamma\text{-}1,2\text{-}H_2SiV_2W_{10}O_{40}]^{4-} + H_2O + \text{epoxide} \quad (1)$$

at the same level of theory. For this purpose, we calculate geometries and energies of all structures presented in Scheme 1.

II. Computational Details

Methods. All calculations were performed using the Gaussian 03 program.[13] The geometries of all species under investigation were optimized without any symmetry constraint at the B3LYP/Lanl2dz level of theory with additional d polarization functions for Si atom ($\alpha = 0.55$) and the corresponding Hay−Wadt effective core potential (ECP) for W and V.[14,15] This approach is subsequently referred to as B3LYP/[Lanl2dz + d(Si)]. The energies of the optimized structures were further refined by performing single-point calculations with the Stuttgart group's pseudopotentials[16] and associated SDD basis sets for W and V and the standard 6−31+G* split-valence basis set for all other atoms. This approach will be referred subsequently to as B3LYP/SDD.

Hessians at some transition states were confirmed to have one imaginary frequency corresponding to the reaction coordinates. However, because of the large size of models used in this study, it was not technically possible to calculate Hessians for all reported structures. The dielectric effects from the surrounding environment were estimated using the self-consistent reaction field IEF-PCM method[17] at the B3LYP/[Lanl2dz+d(Si)] level. As in the reported experiments, acetonitrile was used as a solvent (dielectric constant (ε) = 36.64). Below, we discuss gas-phase energetics calculated at the B3LYP/SDD level of theory. The energies including solvent effects are provided in parentheses. The Cartesian coordinates of all optimized structures at the B3LYP/[Lanl2dz + d(Si)] level of theory are presented in the Supporting Information.

One should note that the structures and energetics of the intermediates and transition states of "peroxo" pathway of the reaction 1 were also calculated by Mizuno and co-workers at the DFT level.[11] However, to be able to compare the "peroxo" and "hydroperoxo" pathways of reaction 1 at the same level of theory, here we also reinvestigate the "peroxo" pathway of this reaction at the B3LYP/SDD level of theory used throughout this paper.

Models. C_2H_4 was used to model an olefin, and H_2O_2 was utilized as an oxidant. As a catalyst we used full structures of the experimentally reported complexes excluding countercations. Compound **I** was isolated[6,11] as the *n*-tetrabutylammonium (TBA) (n-Bu_4N^+) salt, which is a large countercation and its explicit inclusion into calculations is technically impossible; therefore, tetramethylammonium ion (Me_4N^+) was used to model the n-Bu_4N^+ countercation. We have evaluated the role of the countercation only in the rate-limiting steps of the proposed mechanisms by re-optimizing geometries and calculating energies of pre-reaction complexes and corresponding transition states by explicitly including one countercation (Me_4N^+) into the calculations. The position of the countercation in the $\{[\gamma\text{-}1,2\text{-}H_2SiV_2W_{10}O_{40}]^{4-}\}$-($Me_4N^+$) adduct was optimized by placing (Me_4N^+) at different positions around the Keggin cage. It was found that the structure where (Me_4N^+) is located in the vicinity of the V-centers is energetically the most stable one. The structure with (Me_4N^+) at the opposite (relative to the V-centers) position is 12.4 kcal/mol less stable. Therefore, below we discuss only the structures where (Me_4N^+) is located in the vicinity of the V-centers. Below, energies of the structures with a countercation will be presented in brackets (numbers given without parentheses are gas-phase data, while the numbers given in parentheses include solvent effects).

An overall charge of the studied structures (without a countercation) was chosen to be −4, and as shown previously, they have a singlet ground electronic state.[11,18] At the present level of theory, the modeled overall epoxidation process, eq 2, was calculated to be exothermic by 46.8 (47.1) kcal/mol versus the experimental value of 50.3 kcal/mol[19]

$$C_2H_4 + H_2O_2 \rightarrow C_2H_4O + H_2O \quad (2)$$

III. Results and Discussion

A. Formation of Hydroperoxo Intermediate. As seen in Scheme 1, the initial step of both the "hydroperoxo" and

(5) (a) Grigoropoulou, G.; Clark, J. H.; Elings, J. A. *Green Chem.* **2003**, *5*, 1–7. (b) Noyori, R.; Aoki, M.; Sato, K. *Chem. Commun.* **2003**, 1977–1986. (c) Arends, I. W. C. E.; Sheldon, R. A. *Top. Catal.* **2002**, *19*, 133–141. (d) Wei, D.; Chuei, W.; Haller, G. L. *Catal. Today* **1999**, *51*, 501–511. (e) Schuchardt, U.; Guerreiro, M. C.; Shul'pin, G. B. *Russ. Chem. Bull.* **1998**, *47*, 247–252. (f) Neumann, R.; Levin-Elad, M. *Appl. Catal., A* **1995**, *122*, 85–97. (g) Bellussi, G.; Rigutto, M. S. *Stud. Surf. Sci. Catal.* **1994**, *85*, 177–213. (h) Bortolini, O.; Di Furia, F.; Scrimin, P.; Modena, G. *J. Mol. Catal.* **1980**, *7*, 59–74. (i) Eisenbraun, E. J.; Bader, A. R.; Polacheck, J. W.; Reif, E. *J. Org. Chem.* **1963**, *28*, 2057–2062. (j) Bolm, C. *Coord. Chem. Rev.* **2003**, *237*, 245–256. (k) Conte, V.; Di Furia, F.; Licini, G. *Appl. Catal., A* **1997**, *157*, 335–361. (l) Crans, D. C.; Smee, J. J.; Gaidamauskas, E.; Yang, L. *Chem. Rev.* **2004**, *104*, 849–902. (m) Rehder, D. *Inorg. Chem. Commun.* **2003**, *6*, 604–617. (n) Butler, A. *Coord. Chem. Rev.* **1999**, *187*, 17–35. (o) Butler, A.; Walker, J. V. *Chem. Rev.* **1993**, *93*, 1937–1944. (p) Hirao, T. *Coord. Chem. Rev.* **2003**, *237*, 1. (q) Hirao, T. *Chem. Rev.* **1997**, *97*, 2707–2724. (r) Shilov, A. E.; Shul'pin, G. B. *Chem. Rev.* **1997**, *97*, 2879–2932. (s) Thematic issue on vanadium-based catalysts for the selective oxidation of hydrocarbons and their derivatives: *Appl. Catal., A* **1997**, *157*, 1−425; (t) Sigel, H.; Sigel, A. *Vanadium and Its Role in Life*; Marcel Dekker: New York, 1995; (u) Jiang, F.; Anderson, O. P.; Miller, S. M.; Chen, J.; Mahroof-Tahir, M.; Crans, D. C. *Inorg. Chem.* **1998**, *37*, 5439–5451. (v) Butler, A.; Clague, M. J.; Meister, G. E. *Chem. Rev.* **1994**, *94*, 625–638. (w) Ligtenbarg, A. G. J.; Hage, R.; Feringa, B. L. *Coord. Chem. Rev.* **2003**, *237*, 89–101. (x) Khenkin, A. M.; Weiner, L.; Wang, Y.; Neumann, R. *J. Am. Chem. Soc.* **2001**, *123*, 8531–8542. (y) Gall, R. D.; Faraj, M.; Hill, C. L. *Inorg. Chem.* **1994**, *33*, 5015–5021.

(6) Nakagawa, Y.; Kamata, K.; Kotani, M.; Yamaguchi, K.; Mizuno, N. *Angew. Chem., Int. Ed.* **2005**, *44*, 5136–5141.

(7) Nakagawa, Y.; Uehara, K.; Mizuno, N. *Inorg. Chem.* **2005**, *44*, 14–16.

(8) Nakagawa, Y.; Uehara, K.; Mizuno, N. *Inorg. Chem.* **2005**, *44*, 9068–9075.

(9) Mizuno, N.; Nakagawa, Y.; Yamaguchi, K. *J. Mol. Catal. A* **2006**, *251*, 286–290.

(10) Mizuno, N.; Yamaguchi, K. *Chem. Rec.* **2006**, *6*, 12–22.

(11) Nakagawa, Y.; Mizuno, N. *Inorg. Chem.* **2007**, *46*, 1727–1736.

(12) Prabhakar, R.; Morokuma, K.; Hill, C. L.; Musaev, D. G. *Inorg. Chem.* **2006**, *45*, 5703–5709.

(13) Frisch, M. J. et al. *Gaussian 03*, Revision C1; Gaussian, Inc.: Wallingford, CT, 2004.

(14) (a) Becke, A. D. *Phys. Rev. A* **1988**, *38*, 3098–3107. (b) Lee, C.; Yang, W.; Parr, R. G. *Phys. Rev. B* **1988**, *37*, 785–789. (c) Becke, A. D. *J. Chem. Phys.* **1993**, *98*, 1372–1380.

(15) (a) Hay, P. J.; Wadt, W. R. *J. Chem. Phys.* **1985**, *82*, 270–283. (b) Hay, P. J.; Wadt, W. R. *J. Chem. Phys.* **1985**, *82*, 299–310. (c) Wadt, W. R.; Hay, P. J. *J. Chem. Phys.* **1985**, *82*, 284–298.

(16) Andrae, D.; Häuβermann, U.; Dolg, M.; Stoll, H.; Preuss, H. *Theor. Chim. Acta* **1990**, *77*, 123–141.

(17) Cances, E.; Mennucci, B.; Tomasi, J. *J. Chem. Phys.* **1997**, *107*, 3032–3041.

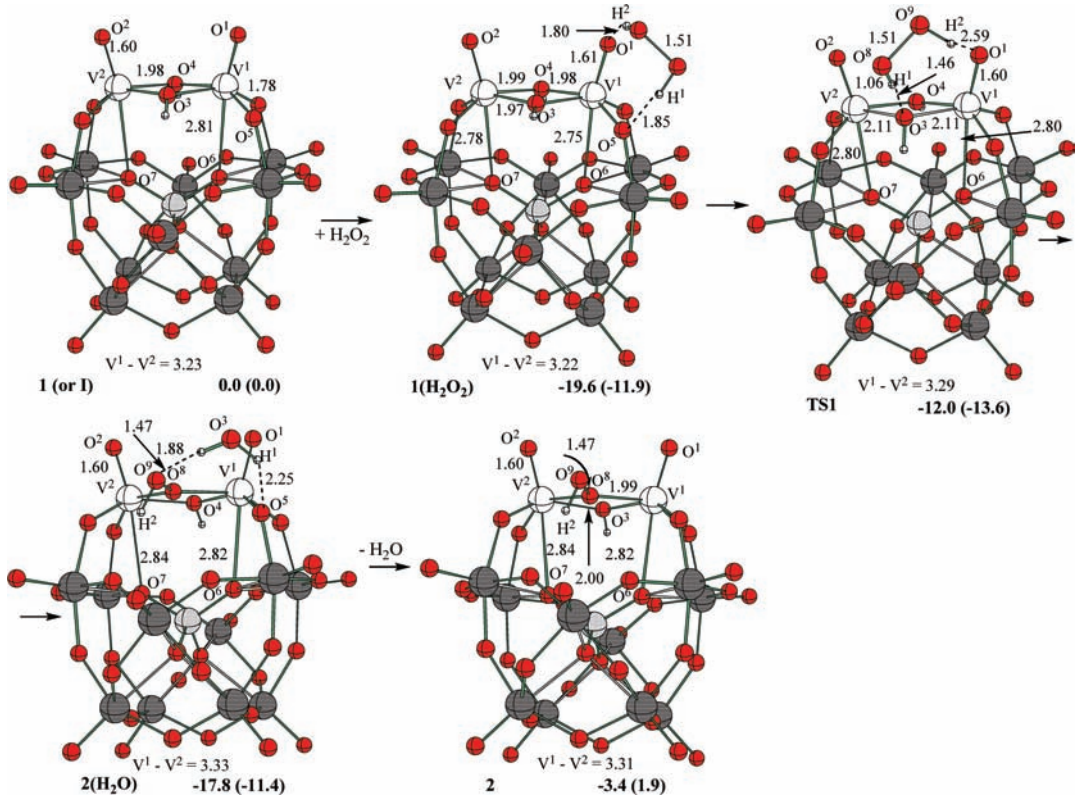

Figure 1. Calculated structures, important geometry parameters (distances in Å, angles in deg), and relative energies (in kcal/mol) of the reactants, intermediates, transition state, and products of the reaction {OV-(μ-OH)$_2$-VO}, **1** + H_2O_2 → {OV-(μ-OH)(μ-OOH)-VO}(H_2O), **2(H$_2$O)** → {OV-(μ-OH)(μ-OOH)-VO}, **2** + H_2O.

"peroxo" mechanisms of the reaction 1 is the same, namely, the coordination of H_2O_2 to the catalyst and the formation of hydroperoxo intermediate, **2**, with an {OV-(μ-OOH)(μ-OH)-VO} core:

$$\{\text{OV-}(\mu\text{-OH})_2\text{-VO}\},\mathbf{1} + H_2O_2 \rightarrow \{\text{OV-}(\mu\text{-OOH})(\mu\text{-OH})\text{-VO}\}(H_2O),\mathbf{2} \quad (3)$$

Important geometry parameters of the reactant, intermediate, transition state, and product of the reaction 3, with or without extra water molecule, are given in Figure 1 (while all their optimized structures are given in the Supporting Information).

As it could be expected, the first intermediate of this reaction is the **1(H$_2$O$_2$)** complex, where the oxidant species H_2O_2 forms hydrogen bonds with the oxygen atoms of $V^1{=}O^1$ and $V^1{-}O^5$ bonds of the catalyst **1**; the calculated $O^1{-}H^2$ and $O^5{-}H^1$ distances are 1.80 and 1.85 Å, respectively. The bonding energy between **1** and **H$_2$O$_2$** is found to be 19.6 (11.9) kcal/mol.

From the structure **1(H$_2$O$_2$)**, in a concerted manner, the $O^8{-}H^1$ bond of H_2O_2 is broken and the proton is transferred to the hydroxyl group (-O^3H) of the {OV-(μ-OH)$_2$-VO} core of the catalyst. This leads to formation of the -$O^8O^9H^2$ species and a water molecule, H_2O^3. The resulting -$O^8O^9H^2$ attacks the vacant site (created by dissociation of the formed water molecule) on the metal center to generate the vanadium-hydroperoxo structure {O^1V^1-(μ-$O^8O^9H^2$)(μ-OH)-V^2O^2}-(H_2O), **2(H$_2$O)**. This step of the reaction proceeds via a transition state **TS1**, where all the corresponding bond distances (O^8H^1 =1.06 Å, O^3H^1 = 1.46 Å and $V^1{-}O^3H$ = 2.11 Å) indicate the proton migration from H_2O_2 to O^3H and the formation of a water molecule (H_2O^3). It is noteworthy that, in comparison to **1(H$_2$O$_2$)**, in **TS1**, $V^1{-}O^3$ and $V^2{-}O^3$ bond distances are elongated by 0.14 Å to facilitate the formation and release of the water molecule. During the reaction **1(H$_2$O$_2$)** → **TS1** → **2(H$_2$O)**, both $V^1{-}V^2$ and $V^1{-}O^6$ bond distances are increased continuously, i.e., 3.22 Å < 3.29 Å < 3.33 Å and 2.75 Å < 2.80 Å <2.82 Å, respectively. As seen in Figure 1, formation of the vanadium-hydroperoxo species, {O^1V^1-(μ-$O^8O^9H^2$)(μ-OH)-V^2O^2}-(H_2O), **2(H$_2$O)**, from **1(H$_2$O$_2$)** is a slightly endothermic process, by 1.8 (0.5) kcal/mol, and proceeds without a barrier in solution but with a 7.6 kcal/mol barrier in the gas-phase (the calculated energy difference between transition state **TS1** and **1(H$_2$O$_2$)** is 7.6 (−1.7) kcal/mol).

The overall reaction 3 is calculated to be 17.8 (11.4) kcal/mol exothermic. Dissociation of water molecule from **2(H$_2$O)** requires 14.4 (13.3) kcal/mol energy, i.e., reaction **1** + H_2O_2 → **2** + H_2O is calculated to be exothermic by only 3.4 kcal/mol in the gas-phase. In the acetonitrile solvent, it is (1.9) kcal/mol endothermic. Thus, the formation of **2** + **H$_2$O** from **1** and H_2O_2 is a facile process. Our conclusion and the

(18) Prabhakar, R.; Morokuma, K.; Geletii, Y. V.; Hill, C. L.; Musaev, D. G. *Computational Modeling for Homogenous and Enzymatic Catalysis;* Musaev, D. G.; Morokuma, K., Eds.; Wiley-VCH Verlag GmbH & Co: New York, 2008, p. 215.
(19) CRCHandbook of Chemistry and Physics; Lide, D. R.; Frederikse, H. P. R. , *Eds.*; CRC Press: Boca Raton, FL, New York, London, Tokyo, 2005.

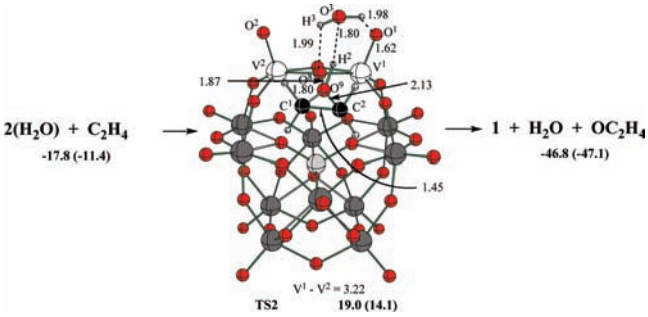

Figure 2. Calculated O-atom transfer transition state, its important geometry parameters (distances in Å, angles in deg.), and associated energies (in kcal/mol) of the "hydroperoxo" pathway of the reaction [γ-1,2-$H_2SiV_2W_{10}O_{40}$]$^{4-}$ + H_2O_2 + Olefin → [γ-1,2-$H_2SiV_2W_{10}O_{40}$]$^{4-}$ + H_2O + Epoxide.

calculated exothermicity of the reaction **1** + H_2O_2 → **2** + H_2O are in an excellent agreement with the finding of Nakagawa and Mizuno.[11]

One should note that the calculated 14.4 (13.3) kcal/mol **2--H_2O** interaction energy in **2(H_2O)** looks slightly overestimated because of the lack of the countercation effect in these calculations. Indeed, the inclusion of the countercation into calculations reduces this energy to [4.8] [(9.1)] kcal/mol. This could be ascribed to the decrease of the Mulliken charges on the O^9 and $O_{(V-O-W)}$ atoms to which H_2O molecule coordinates (see Figure 3) upon the coordination of the countercation to **2**.

From the intermediates {O^1V^1-(μ-$O^8O^9H^2$)(μ-OH)-V^2O^2}-(H_2O), **2(H_2O)**, and **2** reaction may proceed via two distinct pathways: "hydroperoxo" and "peroxo". Below, we discuss these pathways separately.

B. Hydroperoxo Pathway. For the reaction to proceed via this pathway it should start from the intermediate {O^1V^1-(μ-$O^8O^9H^2$)(μ-OH)-V^2O^2}(H_2O), **2(H_2O)**, rather than the intermediate **2.** Our preliminary studies[18] indicate that the presence of a water molecule in the vicinity of the active species with the {O^1V^1-(μ-$O^8O^9H^2$)(μ-OH)-V^2O^2} core is absolutely necessary. Therefore, here we only report the "hydroperoxo" pathway that starts from **2(H_2O)**, which adds the C_2H_4 substrate and produces ethylene epoxide ($C_2H_4O^9$):

$$\{O^1V^1\text{-}(\mu\text{-}O^8O^9H^2)(\mu\text{-}OH)\text{-}V^2O^2\}(H_2O)+C_2H_4 \rightarrow \{O^1V^1\text{-}(\mu\text{-}O^8H^2)(\mu\text{-}OH)\text{-}V^2O^2\}(H_2O)+C_2H_4O^9 \quad (4)$$

During this reaction, the O^9-H^2 bond of the μ-$O^8O^9H^2$ species is broken in a concerted fashion, and the proton is transferred through a water molecule (produced in reaction (3)) to the O-atom bound to the two vanadium centers (μ-O^8) (see Figure 2). It proceeds with a 36.8 (25.5) kcal/mol energy barrier (calculated from the intermediate **2(H_2O)**) at the transition state **TS2**. The calculated energy difference between **TS2** and the reactants (**1** + H_2O_2 + C_2H_4) is 19.0 (14.1) kcal/mol. All the calculated bond distances (O^9H^2 =1.07 Å, O^3H^2 =1.80 Å, and O^8-O^9=1.87 Å) associated with the reaction coordinate indicate that this is a synchronous process. In **TS2**, in comparison to **2(H_2O)**, V^1-O^8, V^2-O^8 and the metal−metal (V^1-V^2) bond distances are shrunk by 0.08 Å, 0.07 Å, and 0.08 Å, respectively. The formation of ethylene epoxide from **2(H_2O)** and ethylene molecule is found to be exothermic by 29.0 (35.7) kcal/mol.

Comparison of the calculated energies in the gas-phase and solution-phase shows that the inclusion of solvent effects at the IEF-PCM level, using CH_3CN as a solvent, significantly changes the calculated energies of the reaction 4. It reduces the barrier for epoxidation at **TS2** from 36.8 kcal/mol to (25.5) kcal/mol and increases the reaction energy from 29.0 to (35.7) kcal/mol.

However, these energies of the reaction **1** + H_2O_2 →... → **2(H_2O)** → **TS2** →... do not include the effects of a countercation; as mentioned above, in the experiment[6] the compound **1** was isolated as a salt of tetra-*n*-butylammonium ion (*n*-Bu_4N^+). To estimate the effects from one countercation (previously, we have shown that inclusion of the *first* countercation molecule into calculations has the most pronounced effect on the calculated energetics and geometries[12,18]) on the calculated barrier of the O-atom transfer from **2(H_2O)** to olefin we explicitly include Me_4N^+ (model of *n*-Bu_4N^+) into calculations of the structures and energetics of **2(H_2O)** and **TS2**. Geometry of the pre-reaction complex **2(H_2O)** was fully optimized in the presence of one molecule of Me_4N^+ (structure **2(H_2O)$_{1CC}$**, Figure 3). However, during the optimization of the transition state structure **TS2$_{1CC}$**, the main reaction coordinates (O^8-O^9, O^9-H^2, O^3-H^2, O^9-C^1, and O^9-C^2 bond distances) are kept frozen at their gas-phase values, but all other parameters were optimized. One should note that the position of the countercation around the POM-cage is determined by electrostatic interaction between the fragments. For example, analysis of the Mulliken charges on the POM-cage of **2(H_2O)** shows that oxygens of O=W groups bear more negative charge (−0.71e) than those of O=V groups (−0.53e). Therefore, the optimized structures of ion-pairs, presented in this paper, where the countercation is located in the vicinity of V=O groups, should be considered as local minima. However, since we investigate reactions occurring in the vicinity of V=O groups, we feel that these local minima of ion-pairs suit much better for our purposes than global minima where the countercation could be located on the opposite (relative to V=O groups) side of the cage.

Solvent effects are included in the calculated energetics by performing single-point IEF-PCM (using CH_3CN as a solvent) calculations of the optimized **2$_{1CC}$** and **TS2$_{1CC}$** structures. As seen from Figure 3, inclusion of Me_4N^+ into calculations makes the barrier for epoxidation to be [31.7][(21.6)] kcal/mol, i.e., reduces it by [5.1][(3.9)] kcal/mol. This could be a result of strong interaction between the countercation Me_4N^+ and the POM-cage and charge redistribution between them. Indeed, the calculated **2(H_2O)**---Me_4N^+ bonding energy is very large, 185.9 kcal/mol, in the gas-phase but reduces to (16.7) kcal/mol in solution, which is still substantial.

One should note that the optimization of the geometries of the **1**—Me_4N^+ ion-pair in solution (using CH_3CN as a solvent) at the IEF-PCM level only slightly changed the energies and geometries of the system.

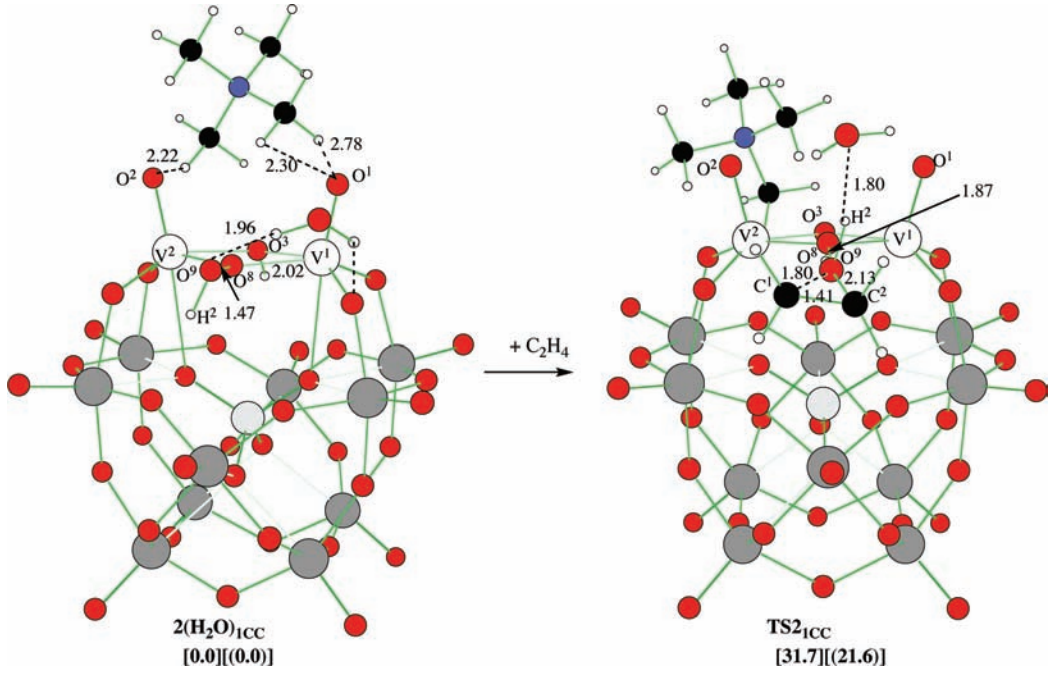

Figure 3. Calculated pre-reaction complex and O-atom transfer transition state of the "hydroperoxo" pathway of the $[\gamma\text{-}1,2\text{-}H_2SiV_2W_{10}O_{40}]^{4-}$ + H_2O_2 + Olefin → $[\gamma\text{-}1,2\text{-}H_2SiV_2W_{10}O_{40}]^{4-}$ + H_2O + Epoxide with one Me_4N^+ countercation included into calculations. Important geometry parameters (distances in Å, angles in deg) and associated energies (in kcal/mol) of the related structures are also presented.

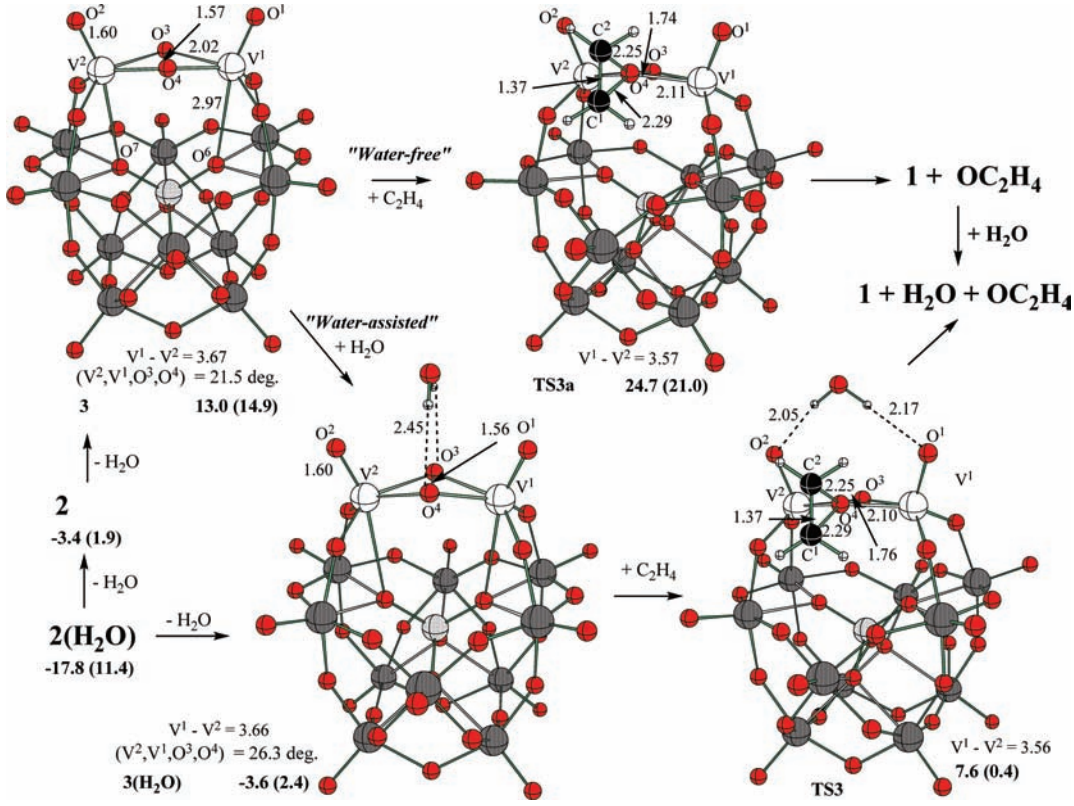

Figure 4. Calculated intermediates and transition states of the "peroxo" pathways of the reaction $[\gamma\text{-}1,2\text{-}H_2SiV_2W_{10}O_{40}]^{4-}$ + H_2O_2 + Olefin → $[\gamma\text{-}1,2\text{-}H_2SiV_2W_{10}O_{40}]^{4-}$ + H_2O + Epoxide. Important geometry parameters (distances in Å, angles in deg) and associated energies (in kcal/mol) of the related structures are also presented.

C. Peroxo Pathways. As mentioned above, the peroxo pathways start from the same intermediates, **2(H_2O)** and **2**, as the hydroperoxo pathway but proceed via the formation of peroxo intermediates **3(H_2O)** and **3**, respectively, with the {OV-(η^2-O_2)-VO} core (see Figure 4). Formation of **3** was experimentally reported by Nakagawa and Mizuno[11] and was proposed to be an active oxidant species of the $[\gamma\text{-}1,2\text{-}H_2SiV_2W_{10}O_{40}]^{4-}$-catalyzed olefin epoxidation by hydrogen peroxide. In general, the first steps of the peroxo pathways, the **2(H_2O)** → **3(H_2O)** and **2** → **3** hydroperoxo → peroxo rearrangements are very complex processes and believed to occur via the protonation of OOH but deprotonation of OH

fragments of **2(H$_2$O)** and **2** by surrounding solvent molecules. This assumption is in good agreement with the experimental observations showing no formation of **3** in the aprotic solvents.[11] It is almost impossible to accurately calculate these protonation and deprotonation steps. Therefore, here we did not calculate any barriers associated with this process. However, we did estimate thermodynamicity of the **2** → **3** and the **2(H$_2$O)** → **3(H$_2$O)** processes, which are found to be 16.4 (13.0) and 14.2 (9.0) kcal/mol endothermic, respectively. Comparison of these calculated energetics shows that the presence of a water molecule in the vicinity of the vanadium-centers slightly reduces endothermicity of the hydroperoxo → peroxo rearrangement step. One should note that the calculated endothermicity of the **2** → **3** rearrangement agrees well with the about 17.0 kcal/mol reported by Nakagawa and Muzino.[11]

To estimate the role of the water molecule located in the vicinity of the active species, we have calculated the second step of the peroxo pathways, the O-atom transfer process, starting from the both **3** and **3(H$_2$O)** complexes. Below we refer to the resulting pathways as "water-free" and "water-assisted" peroxo pathways, respectively. One should note that Nakagawa and Mizuno have studied *only* the "water-free peroxo" pathway.

"Water-Free Peroxo" Pathway. This pathway starts from the peroxo species **3** by addition of olefin (C_2H_4). As seen in Figure 4, where we present important geometries of all calculated intermediates and transition states of the peroxo pathways, the O^3-O^4 bond distance in **3** is 1.57 Å, which corresponds to the O−O single bond. Other calculated geometry parameters of **3** are similar to those of **2**, except the V^1-V^2 and V−O(Si) bond distances. Indeed, the V^1-V^2 distance of 3.67 Å in **3** is almost 0.36 Å longer than that in **2**. Similarly, V−O(Si) bond distances of 2.97 Å in **3** are 0.13 Å longer than those in **2**. In other words, **2** → **3** rearrangement facilitates the formation of the "out-of-pocket" structure[20,21] that is expected to be more reactive than "in-pocket" structure with strong (and short) V−O(Si) interactions (bond distances).

Coordination of the substrate (C_2H_4) to one of the oxygen atoms of η^2-O_2 fragment leads to the formation of an epoxide with an 11.7 (6.1) kcal/mol barrier (calculated from the **3** pre-reaction complex) at the transition state **TS3a**. As seen in Figure 4, the activated O^3-O^4 bond distance in **TS3a** is 1.74 Å, which is by 0.17 Å longer than that in the pre-reaction complex **3**. Other broken, V−O and C^1-C^2, bond distances are 2.11 and 1.37 Å, respectively, which are only slightly longer than those in the pre-reaction complex. In other words, the calculated geometry of **TS3a** is closer to that of the pre-reaction complex **3**, and **TS3a** is an early transition state. The reaction **3** → **TS3a** → **I** + OC_2H_4 is calculated to be highly (59.8 (62.0) kcal/mol) exothermic.

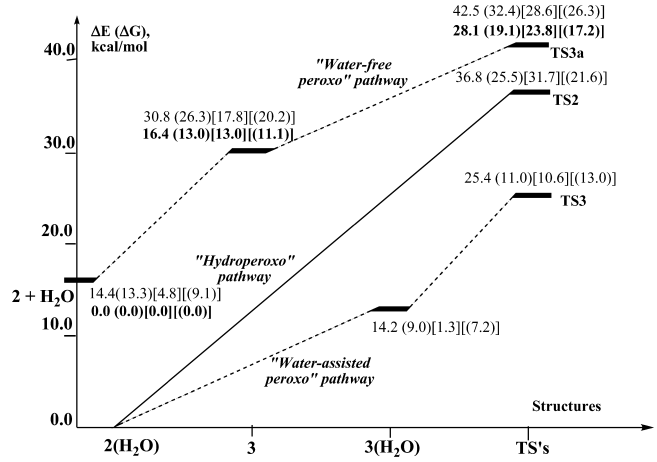

Figure 5. Comparison of relative energies of the "hydroperoxo", "water-free peroxo", and "water-assisted peroxo" pathways of the reaction [γ-1,2-$H_2SiV_2W_{10}O_{40}]^{4-}$ + H_2O_2 + Olefin → [γ-1,2-$H_2SiV_2W_{10}O_{40}]^{4-}$ + H_2O + Epoxide. Numbers given in bold are calculated relative to **2** + H_2O + C_2H_4 reactants, while plain numbers are calculated relative to **2(H$_2$O)** + C_2H_4 reactants.

As mentioned above, the "water-free peroxo" pathway was previously studied by Nakagawa and Mizuno at the DFT level.[11] The reported 11.7 (6.1) kcal/mol barrier and the 59.8 (62.0) kcal/mol exothermicity in the present paper for the reaction **3** → **TS3a** → **I** + OC_2H_4 are in good agreement with about 11.7 and 51.9 kcal/mol reported by Nakagawa and Mizuno.[11]

Comparison of the calculated energies in the gas-phase and solution-phase shows that the inclusion of solvent effects at the IEF-PCM level, using CH_3CN as a solvent, significantly reduces the O-atom transfer barrier at **TS3a** (from 11.7 to 6.1 kcal/mol) but slightly increases the exothermicity of the reaction **3** → **I** + OC_2H_4 (from 59.8 to 62.0 kcal/mol).

However, the aforementioned gas-phase and solution-phase values of the calculated energies of the "water-free peroxo" pathway do not include the countercation effect. To estimate the countercation effect we have re-calculated the pre-reaction complexes **2**, **3**, and transition state **TS3a** in the presence of one Me_4N^+ molecule. These calculations were performed in similar ways as those for **1$_{1CC}$**, **2(H$_2$O)$_{1CC}$**, and **TS2$_{1CC}$**, reported above. The calculated structures of **2$_{1CC}$**, **3$_{1CC}$**, and **TS3a$_{1CC}$** are given in the Supporting Information. Calculations show that the inclusion of the countercation into calculations only slightly changes the O-atom transfer barrier; the O-atom transfer barrier becomes [10.8][(6.1)] kcal/mol at the transition state **TS3a$_{1CC}$**.

"Water-Assisted Peroxo" Pathway. This pathway starts from the peroxo intermediate **3(H$_2$O)**, which uptakes the substrate (C_2H_4) and transfers one of the O atoms of its O_2 unit to the olefin at the transition state **TS3**. This process occurs via an 11.2 (2.0) kcal/mol barrier. Again, inclusion of solvent effects into calculations significantly reduces the O-atom transfer barrier. However, as seen from the data given in Figure 5, inclusion of one countercation (Me_4N^+) molecule into calculations only slightly changes this barrier; the O-atom transfer barrier at the transition state **TS3$_{1CC}$** (see Supporting Information), calculated relative to pre-reaction complex **3(H$_2$O)$_{1CC}$**, is [9.3][(5.8)] kcal/mol.

(20) Botar, B.; Geletii, Y. V.; Kogerler, P.; Musaev, D. G.; Morokuma, K.; Weinstock, I. A.; Hill, C. L. *J. Am. Chem. Soc.* **2006**, *128*, 11268–11277.

(21) Quiñonero, D.; Wang, Y.; Morokuma, K.; Khavrutskii, L. A.; Botar, B.; Geletii, Y. V.; Hill, C. L.; Musaev, D. G. *J. Phys. Chem. B* **2006**, *110*, 170–173.

D. Comparison of Hydroperoxo and Peroxo Mechanisms. Calculated relative energies of the hydroperoxo and peroxo pathways of the targeted reaction are given in Figure 5.

As seen in Figure 5, the presented (water assisted) "hydroperoxo" mechanism of the reaction **2(H$_2$O)** + C_2H_4 → **1** + H_2O + C_2H_4 proceeds with a 36.8(25.5)[31.7][(21.6)] kcal/mol rate-determining barrier at the transition state **TS2 [TS2$_{1CC}$]**. In the meantime, the total energy barrier [involving the hydroperoxo → peroxo rearrangement, **2** → **3**, and the O-atom transfer (at **TS3a**) steps] required for the "water-free peroxo" mechanism is 28.1(19.1)[23.8][(17.2)] kcal/mol, which is smaller than that required for the "hydroperoxo" pathway. Another peroxo pathway, called "water-assisted peroxo" pathway, has even smaller overall energy barrier, only 25.4(11.0)[10.6][(13.0)].

Comparison of the overall energy barriers required for the "hydroperoxo", "water-free peroxo", and "water-assisted peroxo", pathways shows that the proposed peroxo pathways of the **1**-catalyzed olefin epoxidation reaction are more feasible than the "hydroperoxo" pathway. Between the two different peroxo mechanisms, the most favorable is the "water-assisted peroxo" pathway. On the basis of these results, we conclude that the [γ-1,2-$H_2SiV_2W_{10}O_{40}$]$^{4-}$-catalyzed olefin epoxidation by H_2O_2, reported by Nakagawa and Mizuno,[6,11] most likely occurs via a "water-assisted peroxo" mechanism. Furthermore, the rate-determining step of the overall reaction **1** + H_2O_2 + C_2H_4 → **1** + H_2O + OC_2H_4 is the hydroperoxo → peroxo rearrangement step. Solvent (water and acetonitrile) and countercations facilitate the overall reaction.

IV. Conclusions

From the above presented data we can draw the following conclusions.

(1) The formation of the vanadium-hydroperoxo species **2(H$_2$O)** with the {OV-(μ-OOH)(μ-OH)-VO}(H_2O) core from the [γ-1,2-$H_2SiV_2W_{10}O_{40}$]$^{4-}$, **1** (or **I**), and hydrogen peroxide is a facile process, which, most likely, occurs without an energy barrier. It is exothermic by 17.8 (11.4) kcal/mol. The resulting **2(H$_2$O)** intermediate may release a water molecule to form complex **2**. The overall reaction of **1** + H_2O_2 → **2** + H_2O is calculated to be exothermic by 3.4 kcal/mol in gas-phase, but it is endothermic by (1.9) kcal/mol in acetonitrile. This conclusion is in an excellent agreement with the experimental and computational findings of Nakagawa and Mizuno.[11]

(2) From the intermediates **2(H$_2$O)** or **2** reaction may proceed via two distinct pathways named as "hydroperoxo" and "peroxo", respectively. The "hydroperoxo" pathway (water-assisted) starts with coordination of olefin (C_2H_4) to **2(H$_2$O)**, proceeds with a 36.8(25.5)[31.7][(21.6)] kcal/mol rate-determining barrier at the O-atom transfer transition state **TS2 [TS2$_{1CC}$]**, and is unlikely to compete with the peroxo pathways.

(3) The "water-free peroxo" and "water-assisted peroxo" pathways start with the rearrangement of the hydroperoxo species **2** and **2(H$_2$O)** to the peroxo species **3** and **3(H$_2$O)**, respectively, with the {OV-(η^2-O_2)-VO} core. This hydroperoxo → peroxo rearrangement is calculated to be endothermic by 16.4(13.0)[13.0][(11.1)] and 14.2(9.0)[1.3][(7.2)] kcal/mol for **2** → **3** and **2(H$_2$O)** → **3(H$_2$O)**, respectively. Reported endothermicity of the hydroperoxo → peroxo rearrangement is in good agreement with the experimental observations showing no formation of **3** in the aprotic solvents.[11]

(4) Among the peroxo mechanisms the "water-assisted peroxo" pathway occurs with the lesser overall energy barrier, only 25.4(11.0)[10.6][(13.0)] kcal/mol compared to 28.1(19.1)[23.8][(17.2)] kcal/mol for "water-free peroxo" pathway, and expected to be a favorable pathway of the **1**-catalyzed olefin epoxidation reaction. The rate-determining step of the overall reaction **1** + H_2O_2 + C_2H_4 → **1** + H_2O + OC_2H_4, which occurs via the "water-free peroxo" pathway, is the hydroperoxo → peroxo rearrangement step. Solvent (water and acetonitrile) and countercations facilitate the overall reaction.

Acknowledgment. The present research is supported by Grant DE-FG02-03ER15461 from the Department of Energy. The use of computational resources at the Cherry Emerson Center for Scientific Computation is also acknowledged.

Supporting Information Available: Completed ref 13, cartesian coordinates of all structures discussed in the paper, and PCM optimized structure of the **1**-Me_4N^+ ion-pair. This material is available free of charge via the Internet at http://pubs.acs.org.

IC801372J